UC Davis

UC Davis Previously Published Works

Title

Data-Driven Approach to Modeling Microfabricated Chemical Sensor Manufacturing

Permalink

https://escholarship.org/uc/item/7fm0z648

Journal

Analytical Chemistry, 96(1)

ISSN

0003-2700

Authors

Chew, Bradley S

Trinh, Nhi N

Koch, Dylan T

et al.

Publication Date

2024-01-09

DOI

10.1021/acs.analchem.3c04394

Peer reviewed

eScholarship.org Powered by the California Digital Library
University of California

Author Manuscript

Author Manuscript

Author Manuscript

Author Manuscript

HHS Public Access

Author manuscript

Anal Chem. Author manuscript; available in PMC 2025 January 09.

Published in final edited form as:

Anal Chem. 2024 January 09; 96(1): 364–372. doi:10.1021/acs.analchem.3c04394.

A Data Driven Approach to Modeling Microfabricated Chemical Sensor Manufacturing

Bradley S. Chew[1,4], **Nhi N. Trinh**[2,4], **Dylan T. Koch**[3,4], **Eva Borras**[1,4], **Michael K. Levasseur**[1,4], **Leslie A. Simms**[1,4], **Mitchell M. McCartney**[1,4,5], **Patrick Gibson**[1,4], **Nicholas J. Kenyon**[4,5,6], **Cristina E. Davis**[1,4,5,*]

[1]Department of Mechanical and Aerospace Engineering, One Shields Avenue, University of California Davis, Davis, CA 95616

[2]Department of Biomedical Engineering, One Shields Avenue, University of California Davis, Davis, CA 95616

[3]Department of Electrical and Computer Engineering, One Shields Avenue, University of California Davis, Davis, CA 95616

[4]UC Davis Lung Center, One Shields Avenue, University of California Davis, Davis, CA 95616

[5]VA Northern California Health Care System, 10535 Hospital Way, Mather, CA 95655

[6]Department of Internal Medicine, 4150 V Street, University of California Davis, Sacramento, CA 95817

Abstract

We have developed a statistical model-based approach to the quality analysis (QA) and quality control (QC) of a gas micro preconcentrator chip (μPC) performance when manufactured at scale for chemical and biochemical analysis of volatile organic compounds (VOCs). To test the proposed model, a medium-sized, university-led production batch of 30 wafers of chips were subjected to rigorous chemical performance testing. We quantitatively report the outcomes of each manufacturing process step leading up to the final functional chemical sensor chip. We implemented a principal component analysis (PCA) model to score individual chip chemical performance, and we observed the first 2 principal components represent 74.28% of chemical testing variance with 111 of 118 viable chips falling into the 95% confidence interval. Chemical performance scores and chip manufacturing data were analyzed using a multivariate regression model to determine the most influential manufacturing parameters and steps. In our analysis, we find the amount of sorbent mass present in the chip (variable importance score = 2.6) and heater and RTD resistance values (variable importance score = 1.1) to be the manufacturing parameters with the most impact on chemical performance. Other non-obvious latent manufacturing

*Corresponding author: cedavis@ucdavis.edu.

SUPPORTING INFORMATION

Supporting information available: The following files are available free of charge.

Supplemental_06: Detailed microfabrication recipes, instrument calibration, CAD drawings for custom equipment, manufacturer analysis reports.

The authors declare the following competing financial interest(s): There are two issued patents on part of the work presented in this paper.

Author Manuscript Author Manuscript Author Manuscript Author Manuscript

parameters also had quantified influence. Statistical distributions for each manufacturing step will allow future large-scale production runs to be statistically sampled during production to perform QA/QC in a real-time environment. We report this study as the first data-driven, model-based production of a microfabricated chemical sensor.

Graphical Abstract

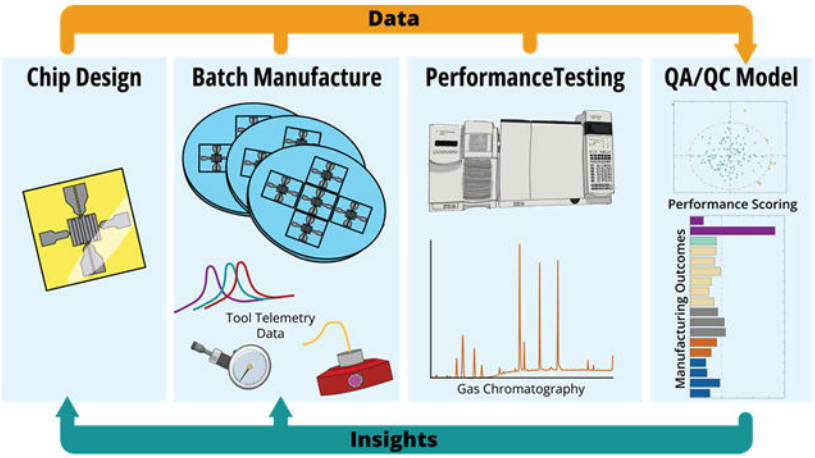

Keywords

Micro preconcentrator; volatile organic compounds (VOCs); exhaled breath volatiles; thermal desorption; MEMS; glass

Chemical sensors and samplers have long been an area of interest for the microelectromechanical system (MEMS) community. Recently, the demand for wearable technologies and point-of-care diagnostic systems coincides with greater research efforts in these areas. Chemical sensors have become increasingly prevalent in therapeutics, tissue engineering, and diagnostics due to its potential of miniaturization and remote sensing [1-4]. These sensors can transduce chemical information, ranging from sample concentration to total compositional analysis. One topic of interest at the cutting edge of human health diagnostics is the study of metabolomics in exhaled breath volatile organic compounds (VOCs) [5-9]. For this application and many others, MEMS transducers must be highly selective and sensitive to chemicals in trace amounts to provide diagnostic data. Improving limits of detection and instrument sensitivity in gas-phase analysis, preconcentration of multi-compound chemical samples is often necessary [10-14]. Preconcentration lowers the limits of volatile detection by collecting a large volume of sample onto a sorbent material, then rapidly thermally desorbing the concentrated sample into a detector.

Our group has previously designed and demonstrated proof-of-concept manufacturing and use of a micro preconcentrator (μPC) [7, 15-18] chip. The μPC is designed to have a hermetically sealed microcavity region filled or coated with a sorbent material to preconcentrate VOCs. There are also connected micro-channels and through-glass vias for gas transport, and metallic patterned heaters and temperature sensors. In operation, a VOC sample can be loaded onto to the sorptive region, and later be rapidly heated to

Author Manuscript Author Manuscript Author Manuscript Author Manuscript

desorb and release the sample from the sorbent into a downstream detection system. In the laboratory, μPC chips can be coupled with chemical sensing platforms such as gas chromatography (GC), mass spectrometry (MS), or in the field to micro differential mobility spectrometers (mDMS) for sample VOC analysis using thermal desorption. As our previous work indicates, μPC chip performance varies depending on several parameters including: adsorption flow, desorption flow, sorbent amount, and thermal management. To date, the relationship between manufacturing process parameters and our μPC chip performance had not been explored.

Scaling chemical sensor manufacturing from one-off proof-of-concept chips to batches in the hundreds or thousands presents a new set of quality assessment (QA) and quality control (QC) challenges. However, overcoming these obstacles enables large scale academic studies like cross-sectional VOC disease fingerprinting and environmental chemical monitoring studies that require chip-to-chip reproducibility. Increasingly, these Quality-By-Design and QA/QC processes are being required by federal funding agencies, such as the National Institutes of Health[19, 20]. In this work, we explore the influence of chip manufacturing parameters on chemical preconcentration performance with the use of statistical methods and multivariate regression modelling of the manufacturing steps. The resulting data allow us to reduce performance variation at the manufacturing level and quantitatively catalog performance variation of every individual chip.

We adapted a prototype chip process [15, 18] into a large batch production run. We present a robust QA/QC manufacturing assessment method based on final chemical performance to depict the uniformity of a high-yield, high uniformity fabrication process of a μPC. For a total of 30 wafer pairs, 150 chips were fabricated with a yield rate of 79.8%. A principal component analysis (PCA) model was built to standardize the chemical performance of μPCs. A partial least squared regression (PLSr) was then used to understand the connections between the chemical performance represented by PCA scores and manufacturing data collected during the process steps. This level of knolwedge on chip variation leads to a method for standardizing an inventory of μPCs for large scale clinical or environmental sampling trials. More broadly, we present a model for scalable MEMS design and manufacturing backed by a QA/QC model including a common set of features, patterned electrodes, micro channels, and sealed cavities ubiquitous to chemical and biological transducers.

MATERIALS AND METHODS

Statistical Parameter Measurements and QA/QC Tracking

Micro Preconcentrator Design.—The μPC (Figure 1) design used as a demonstration in this study consists of a sealed glass cavity with micro-channels and patterned metal heaters and temperature sensors. The requirements of the chip include high temperature and pressure capabilities for chemical analysis, necessitating a robust manufacturing process compatible with glass. The front side of the device contains an integrated heater with two resistance temperature detector (RTD) elements (Figure 1a). The heaters run across the sorbent cavity where power is supplied during desorption to achieve a temperature of 260 °C (Figure 1a, **element 2**). The RTDs surround the edges of the sorbent cavity to allow for

Author Manuscript Author Manuscript Author Manuscript Author Manuscript

temperature monitoring between the sorbent cavity and edges (Figure 1a, **element 4**). Other elements on the front side of the chip include gold contact pads (Figure 1b, **element 1**) for better electrical connection to the electrical components and a quick response (QR) code to easily identify each chip on an individual basis during clinical trials (Figure 1b, **element 3**). There are complimentary etched cavities and channels on both sides of the glass wafers to allow for gas flow and a sorbent to be packed in the cavities (Figure 1a, **elements 4 and 5**). through glass vias on one side of the glass wafer allows for an inlet and outlet to the etched features (Figure 1a, **element 6**). An SEM image shows the feature dimensions of interest in cross-section (Figure 1c). These feature exhibit variations from chip to chip and are measured and reported in our statistical modeling process.

Micro Preconcentrator Manufacturing Process.—The fabrication processes were performed in a Class 100 cleanroom facility (Center for Nano and Micro Manufacturing, UC Davis, CA, USA; Figure 2). Briefly, the process starts with fabricating Figure 1a, elements 4 5 and 6 in 4 in (100 mm) 700 μm thick Borofloat 33 wafer blanks with a topside and backside surface roughness of <1 nm, and warp of <30 μm (University Wafer, South Boston, MA USA). Wafers are etched using laser-initiated deep etching (LIDE) provided as a service from Vitrion (LPKF, Garbsen, Germany) [21]. The cavity, micro channel, and through glass via features are etched nominally to 350 μm with the through glass vias being etched from both sides. The LIDE process was chosen for its ability to render deep, fracture free, high aspect ratio features.

Wafer bonding fuses two complimentary wafers together forming a sealed cavity with through glass vias. Several bonding procedures were considered; fusion, metal eutectic, and anodic bonding [18, 22, 23]. Anodic bonding was chosen as the bonding method for its compatibility with low temperatures, simplicity, and compatibility with conventional IC fabrication [23]. A silicon nitride (SiNx) thin film acts as an intermediate layer between the bonded wafers and is deposited with plasma enhanced chemical vapor deposition (PECVD) using a Plasma-Therm Vision 310 (Plasma-Therm, St. Petersburg, FL, USA).Wafer pairs are aligned and bonded in an EVG 501 (EVG, St. Florian, Austria) wafer bonder at; 400 °C, 550 N compression force, and 1 kV for 3min.

Heating elements and resistive thermal device (RTD) temperature sensors are lithographically patterned tungsten traces. Films of chromium-tungsten-chromium (Cr-W-Cr) were deposited on bonded wafer pairs for 4-35-4 min in an argon environment at a pressure of 5 mTorr with 300 W of in a Lesker Labline Sputter System (Kurt J. Lesker, Jefferson Hills, PA, USA). Conductive traces for heaters and RTDs were lithographically patterned using a negative photoresist, Futurex NR-9 (Futureex Inc., Franklin, NJ, USA), and etched back in alternating Chromium and Tungsten wet etchants (Transene Co Inc., Danvers, MA, USA). Finally, gold film was deposited onto the electrical contact points with a liftoff method using Futurex NR9 photoresist and a CHA E-Beam Evaporator (CHA Industries, Fremont, CA, USA) to improve interface conductivity.

A protective layer of silicon dioxide (SiO2) is patterned over the heating elements and RTDs, leaving only the contact pads exposed. This passivating SiO2 layer prevents trace delamination, and heater degradation during use. Silicon Dioxide is deposited with a

Author Manuscript Author Manuscript Author Manuscript Author Manuscript

Plasma-Therm Vision 310 PECVD tool. The passivation layer is patterned into Futurex NR-78 (Futureex Inc., Franklin, NJ), and etched for 5 min in buffered oxide etchant (BOE 6:1, Sigma-Aldrich, St. Lous, MO, USA).

Before leaving the microfabrication facility, the assembly is annealed [24] in a programmable furnace (Vulcan-Hart 3-550, ESP Chemicals, Tucson, AZ, USA) at 300 °C for 12 hr to improve resistive stability of the heaters over time. Finally, wafers are diced into individual 1in x 1in (25.4mm x 25.4mm) chips with a dicing saw (Disco DAD 312, Disco, Tokyo, Japan)

Sorbent Packing Procedure.—Sorbent material is vacuum packed into the chip cavity and fixed in place with glass wool as described previously [15]. In this demonstration, we used 80/100 mesh Tenax TA (Sigma-Aldrich, St. Lous, MO, USA). Once the cavity is filled with the physical maximum amount of sorbent, glass wool is inserted to prevent the packed sorbent from being expelled during gas flow through the chip.

Fixtures for Chip Analysis.—Custom-made fixtures were manufactured to assist in the calibration and QA/QC assessment of these chips. Microscope clips (SLH2, Thorlabs, Newton, NJ, USA) were used in conjunction with ceramic threaded standoff (94335A370, McMaster-Carr, Elmhurst, IL, USA) with high-temperature compliant bushings to make electrical contact with each of the μPC RTD contact pads. Temperatures were measured with a MAX31865 (Adafruit Industries, New York, NY, USA) temperature sensor amplified and Adafruit Feather M0 Adalogger (Adafruit Industries, New York, NY, USA). RTD measurements were made every 1 s and were simultaneously recorded for batches of 5 chips.

Chemical testing was conducted using an in-house designed aluminum fixture (Figure S1) manufactured by Protolabs (Maple Plain, MN, USA) to interface the μPC chip to the injection port of a gas chromatography oven. The fixture uses precision alignment pins along with two mating aluminum halves to compress a silicon gasket forming a pressure seal around the through glass vias of the chip. A printed circuit board (PCB) manufactured by EasyPCB (Mulina, OR, USA) interfaces surface-mounted pogo pins to a benchtop Agilent E3611A DC Power Supply (Agilent, Santa Clara, CA, USA) and a Keithly 2110 5.5 Digit Multimeter (Keithley Instruments, Cleveland, OH, USA).

Statistical Parameter Measurements and QA/QC Tracking

Manufacturing Parameters.—Tracking each individual chip is essential to the statistical analysis and success of this present study. From the start of production to the end of chemical testing, each chip is individually tracked, and manufacturing parameters are measured at each step. During production and post-production testing, data collected falls into two categories. First, process data from our specific cleanroom instruments are acquired passively during each fabrication step (e.g. PECVD reflected RF, bond charge, bond voltage, bond current, sputter durations, chemical desorption pressure, desorption ramp rate, and desorption temperature). Second, product feature data is intentionally measured after a completed fabrication step and compared to the design value (e.g. channel width, channel depth, thin film thickness, heater resistance, RTD resistance, pad resistance, post-annealing resistances, and sorbent mass). All these measurements are made to attribute sources of

Author Manuscript Author Manuscript Author Manuscript Author Manuscript

variation in chemical preconcentration performance over the statistical population of μPCs in our manufacturing pipeline and to determine specific manufacturing parameters predicting μPC performance.

Etched Feature Parameters.—Etching was inspected with two microscopes to measure channel width and channel depth on both complimentary sides of the. To measure channel width, a Carl Zeiss Axiotron microscope (Carl Zeiss AG, Jena, Germany) set with an objective lens of 10X was equipped with an AmScope MU300 digital camera (AmScope, Irvine, CA, USA) to image the channel. Using an included calibration standard and the AmScope software each channel was measured optically. Depth measurement was conducted on a microscope with an adjustable Z-stage coupled to a Mitutoyo Digimatic (Mitutoyo, Kanagawa, Japan) with ± 0.001 mm of accuracy.

Bonding Feature Parameters.—Silicon nitride intermediate film layer thickness was measured using a J.A. Woollam M-2000 ellipsometer (J.A. Woolam, Lincoln, NE, USA) with the CompleteEase software package. Due to the uniformity of coating in the PECVD process [25-27], one-point measurements at three incident angles (45°, 55°, 65°) were acquired. A model was then selected on CompleteEase preset parameters to determine the SiNx film thickness. To check for any elementary mistakes in the modeling, the refractive index (n), extinction coefficient (k), and mean square error (MSE) were all checked before recording the measurement [28]. During bonding, the entire machine telemetry is automatically recorded by the EVG 501 Wafer Bonder. However, only the electrical properties of the bonder are potentially germane to this study. For an anodic bond, the charge passed through the bonded wafer stack from the electrodes is proportional to bond strength [29]. Total bond charge, maximum voltage, and maximum current were all recorded for later manufacturing statistical analysis.

Heater and RTD Parameters.—After tungsten deposition and pattern etching, both the heaters and RTDs are measured with a Fluke 87V Industrial Multimeter (Fluke Corporation, Everett, WA, USA). Heater resistance is directly related to the metallic film thickness and width of the heater traces, which are outcomes of sputtering thickness and material removal during etching. Resistance values for the Top-RTD, Bottom-RTD, and heater are recorded for later statistical analysis.

Post-Processing Parameters.—Post-processing of each chip occurs outside of a cleanroom environment and prepares the chip for chemical testing. The μPCs are first placed in an oven and heated to 30 °C, followed by a stepwise increase in temperature of 60 °C held for 5 min until a final temperature of 300 °C. At each interval, the resistance values from both RTDs are read and recorded automatically using MAX31865 (Analog Devices, Wilmington, MA, USA) RTD reading integrated circuits. Temperature versus RTD resistance data is used to construct a calibration curve for each chip. During sorbent packing, the μPCs are individually weighed on an analytical balance (Denver Instrument PI-225D Analytical Balance) before and after packing. The mass of sorbent is recorded by calculating the difference between the two values excluding the mass from the glass wool.

Author Manuscript Author Manuscript Author Manuscript Author Manuscript

Chemical Preconcentration Performance Assessment.—The performance of the chip is quantified with a gas chromatography flame ionization detector (GC-FID) (HP 5890 Gas Chromatograph, Hewlett-Packard Development Company, Palo Alto, CA, USA). Preconcentrator chips are fixtured into an aluminum housing with a silicone sealing gasket, incorporating a printed circuit board with pogo pins connecting the preconcentrator electrically to benchtop instrumentation. Before testing, preconcentrators are purged with 40 sccm of ultra-high purity 99.99% nitrogen (UN1066 Nitrogen Compressed) using an Apex mass flow controller (AX-MC-50SCCM-D/5M, 5-in, N2, Apex Vacuum, Woodstock, GA, USA) and set to heat with 2 W of power from a Keithley power supply (Keithly 2200-20-5 DC Power Supply) for 10 min ensuring there are no residual VOC contaminates.

After the initial bakeout, μPCs are allowed to cool to room temperature for an additional 5 min before sampling a TO-15 (Restek TO-15 Subset 25 Component Mix, p/n 36636) VOC gas mixture. After desorption, the calibration VOCs are separated by a GC column (Agilent DB-VRX, 20 m x 0.180 mm diam x 1.00 μm film). The GC method starts at 40 °C for 4 min, then heats from 40 °C to 140 °C at a ramp rate of 10 °C /min, then from 140 °C to 240 °C at a rate of 40 °C/min and holding for 2.5 min. Resulting GC-FID data files are processed by aligning retention times for each sample and integrating peak areas. Chemicals were identified by their Kovat's index and indexing the column with a C7-C30 saturated alkanes solution (C7—C30 Saturated Alkanes certified reference material, Sigma-Aldrich, St. Louis, MO) (Table S1).

RESULTS AND DISCUSSION

Channel etch dimensions were measured for both sides A and B after bonding to capture any distortions incurred by the heating and pressing of the wafers during the process. Figure 3 shows the distributions of the channel width and depth of the two wafer sides with n = 118. The average channel depth including standard error was 314.562 ± 0.645 μm (Figure 3a) and 326.575 ± 0.758 μm (Figure 3b) for side A and B respectively. For channel width, the average and standard error was 709.625 ± 0.089 μm for side A (Figure 3c) and 709.981 ± 0.107 μm for side B (Figure 3d). It was observed that the channel depth was higher for side B as this complimentary wafer had the through-glass vias for gas transport. During the etching step done by Vitrion, side B wafers are etched on both sides successively to achieve the through-glass vias, giving it slightly deeper channels than for side A. Overall we observe channel widths had much tighter tolerances than channel depths, indicating better lateral etch control for this deep glass etching process.

During the bonding process, SiNx was deposited as an intermediate layer between the glass wafers assisting anodic bonding. We show the distribution of the deposited intermediate layer with an average and standard error of 190.277 ± 1.544 nm (Figure 4a), with a total of n = 27. The anodic bonding was performed on the EVG 501 Wafer Bonder where electrical parameters were collected such as maximum voltage, maximum current, and total bond charge. In the EVG 501 Wafer Bonder recipe, the maximum voltage was set to 1000 V, and current was limited up to 15 mA, showing little to no variation in value [23]. However, the total electrical charge had values that ranged from 1807 mC to 2057 mC giving an average and standard error of 1898.2 ± 4.9 mC (Figure 4b). The magnitude of the

Author Manuscript Author Manuscript Author Manuscript Author Manuscript

accumulated electrical charge between the two wafers is used as a nondestructive measure for bond strength [30]. All wafers were successfully bonded showing no signs of excessive substrate cracking, large voids, or incomplete adhesion. Given the high success rate and wide variations for SiNx film thickness and bond charge, the bonding steps appear to have high fabrication variation tolerance.

Resistance values were measured on the heaters, top and bottom RTDs, and gold pads after metal deposition and etching processes were completed. The top and bottom RTDs had values of 115.4 ± 1.9 Ω and 112.8 ± 1.9 Ω respectively, ranging from 69.1 to 168.4 Ω for the top RTDs and 64.4 to 163.8 Ω for the bottom RTDs (Figure 5a, Figure 5b). Heater values also had a range of 149.6 Ω to 283.4 Ω with an average and standard error of 192.7 ± 3.1 Ω (Figure 5c). On each chip, there are six pogo-pin contact pads, giving $n = 708$ where the pads were measured from edge to edge with an average and standard error of 0.8 ± 0.0048 Ω, ranging from 0.1 Ω to 1.3 Ω (Figure 5d). Lower pad resistance and gold coverage contribute to better pogo-pin contact and less electrode error due to positional misalignments for the device while in use.

A conformal passivation layer over the heaters and RTDs was pattered in 650 nm of silicon dioxide. Figure 5e shows the distribution of the measured layer thickness with an average and standard error of 634.64 ± 7.24 nm with a range of 588.46 nm to 713.89 nm. We attribute error in the passivation process to the volume of wafers run successively. During process development deposition rates were calculated using a single wafer at the center of the vacuum chamber. For batch processing, 4 wafers were processed at once distributed evenly throughout the chamber and all 27 wafers were PECVD filmed in one day. Processing in high volume resulted in a buildup of gas-phase nucleation products – particulate debris contaminating the deposition chamber. However, by setting the nominal film thickness to 650 nm even in the minimum deposition case the heaters are encapsulated with silicon dioxide and immune from oxidation while in use.

After device fabrication is complete, in addition to gas chromatography as the primary chemical validation test, we also log desorption pressure and temperature telemetry. In the post-processing of the chip, the μPCs undergo a heating calibration step where the time constant, τ, was calculated for the RTDs, describing how quickly the chips can reach an operating temperature. The calculated τ of the RTDs was 22.37 ± 0.64 s with a range of 11.55 s to 35.64 s (Figure 6a). The range in τ values is a downstream consequence from the variation in RTD resistance values during the etching step of the fabrication process. During chemical desorption, 3 W is supplied to the chip where the maximum RTD temperature can be calculated based on the final resistance value given, evident in Figure 6c giving an average and standard error of 345.36 ± 7.84 °C with a range of 205.54 °C to 542.37 °C. The distribution of the RTD heating profile and maximum RTD temperature both show bimodal tendencies as the values are reliant on each other, emphasizing the importance of having tighter tolerances for the control of parameters impacting resistance, including metallization photolithography and etch control.

Other key parameters measured during post-processing included the mass of sorbent packed into each chip with an average and standard error of 3.08 ± 0.04 mg and range of 1.14

Author Manuscript Author Manuscript Author Manuscript Author Manuscript

mg to 4.22 mg (Figure 6b). The large distribution of sorbent packed into each chip is a consequence of the manual packing process. Expansion of the first glass wool plug after insertion lead to a variable effective cavity volume for sorbent packing. We observed this to be the major contributing effect to the wide distribution in sorbent mass packed.

During chemical testing, pressure over the chip was measured where helium gas is supplied as a carrier gas to the GC-FID. The pressure needed to overcome the 20.0 PSI inlet was measured giving an average and standard error of 39.40 ± 0.001 PSI with a range of 39.10 PSI to 39.64 PSI (Figure 6d). As helium gas was supplied by an Apex mass flow controller (AX-MC-50SCCM-D/5M), a fixed volume of gas flowed through the system where the pressure was monitored to ensure that there were no leaks.

We demonstrate an example chromatogram taken from chip 03C (Figure 7, bottom) focusing on 14 compounds in the mixture. Although each compound in the VOC mixture nominally had the same concentration, small variations in the efficiencies of the detector, column, ionization, and sorbent material, chemical responses were not always equivalent between VOCs. To enhance the comparison of individual VOC responses from all chips, a normalization method was applied by mean centering the data and dividing it by the measurement variation study standard deviation (Equation 1, Figure 7 top).

$$Normalized\ Area = \frac{Peak\ Area - Mean\ Peak\ Area}{Measurement\ Variation\ SD}$$

Variation in chemical response originates from numerous sources, but we sought to isolate chip-to-chip error from variation introduced by the GC-FID system. A measurement variation experiment was conducted by running two chip (n=35 pairs) replicates to quantify variation from the GC-FID and sampling platform. Additionally, the measurement variation normalized data better isolates effects seen in chip-to-chip variation from FID instrument variation while retaining nuances in efficiency for specific compounds that a normalization method like mean centering may omit. The variance for each compound from the measurement variation experiment and chemical performance study for all the chips can be seen in Figure 8.

Demonstrated in Figure 8, for every compound, except for bromodicholoromethane the total variation is larger than the measurement variation. This intuitively represents that the error in the experiment exhibits less variation than that of both the experiment and the chips. More interestingly, the magnitudes for each pair of box plots are similar. We can attribute a large portion of the variation the main study (n=118) to the experimental FID platform, opposed to the preconcentrator chips. This amount of error common for thermal desorption methods [31-33]

A principal component analysis (PCA) was performed followed by a partial least squared (PLS) regression model to devise a model linking manufacturing parameters to a chip performance score.

Author Manuscript Author Manuscript Author Manuscript Author Manuscript

Instead of simply summing peak areas to score chips on chemical performance, PCA was chosen to compress the dimensionality of the chemical test performance data to a single score, while preserving the maximum amount of information from the experiment. By reducing the dimensionality down to an information dense score, a regression model, PLS is applied to find correlations between chip performance and manufacturing tolerances.

The PCA scores in Figure 9a compare the chip-to-chip variation from responses of 14 analyzed compounds. 94% of manufactured μPCs, or 111 chips, fell within the 95% confidence interval. 7 samples fell outside this interval. Notably, 5 out of 7 outliers originated from two wafers. All chips from these wafers had heater resistance and RTD values 46% higher than the mean, and the highest of all manufactured chips. The sputtered thickness of the tungsten layer likely contributed the most to this discrepancy. In an a priori investigation of the sputtering system log files, we discovered the sputtering system had been used the day before to deposit a non-conductive material for an abnormally long duration. In a shared academic fabrication facility, tool cleanliness cannot be controlled to the same degree as in a production facility leading to unforeseen device variation. The abundance of collected data condensed into an easily interpretable model makes pinpointing abnormalities in chip production a streamlined and accurate practice in a production environment. However, this insight illustrates that our data driven process works to identify outliers from the manufacturing processes.

Using the 35 individual variables of data collected throughout the manufacturing process a PLS regression model was constructed to determine the manufacturing parameters most predictive of chemical performance (Figure 9b). To build the model, each chip's PC1 score was used to represent chemical performance. Despite the ability of partial least squares (PLS) regression analysis to account for covariance, only independent manufacturing parameters were selected to select for features immediately actionable with quality control efforts. Predictor variables with a variable importance score (VIP) > 1 are considered to influence the correlation found by the model and are the variables most linked to the outcome of PC1.

From all the studied parameters, sorbent mass packed was the variable with the strongest correlation to the preconcentration performance of the chip represented by PC1. This was an intuitive outcome for the experiment – increased availability of sorbent surface area led to better chemical capture and thus better detector signal. More unexpectedly, heater resistance, and inner RTD resistance were both revealed as variables with correlation to chip performance and were the only microfabrication process variables to show significance in our analysis. Both features of the preconcentrator are fabricated in the same steps, sputtering of tungsten, and in etching with photolithography. Despite operating the heaters at the same wattage, what this may indicate is that certain morphologies of the heaters whether they are slightly thinner or thicker tungsten thickness, wider or narrower etching are more efficient at quickly desorbing the sample, providing a faster burst of chemical for the GC to resolve. No matter the mechanistic cause of the issue, these experimental results prompt secondary experimentation for chip optimization. Compressing high dimensionality data commonplace in a microfabrication setting with our statistical modeling chain highlights two valuable aspects of data-driven manufacturing. First, to confirm presumed problem areas

Author Manuscript Author Manuscript Author Manuscript Author Manuscript

in manufacturing with quantifiable metrics, and second to uncover other areas overlooked by engineering design and analysis.

CONCLUSIONS

In this study, we successfully devised a scalable performance assessment process for the fabrication of micro preconcentrator chips at the wafer level. We also predict this process shares a feature set with other BioMEMS devices and will be translatable to the fabrication of other novel chemical sensors. For this fabrication process, we quantify the variability in each manufacturing process step. Chemically testing the chips, we quantify the performance with GC-FID analysis of a commercial TO-15 multipart gas mixture. In a large batch, n=118 we demonstrate high repeatability for chemical desorption. This was verified with a single chip measurement variation study n=35 to validate the FID instrument variance.

Finally, we present a statistical method for data-driven quality control of a medium to large batch MEMS devices. By using PCA to quantify chip performance and then applying a PLS regression model, we were able to identify physical features of the preconcentrators with the strongest correlation to chip performance. These features in some cases were parameters we suspected were important from the onset of the project, but others were only revealed through advanced modeling analysis. For MEMS devices, where massive amounts of data are passively generated during fabrication or can be actively measured from the production equipment, the final section of this study shows the importance of using engineering design and development skills in combination with advanced statistical and modeling techniques to optimize the performance and yield of a device.

Supplementary Material

Refer to Web version on PubMed Central for supplementary material.

Acknowledgements

This work was partially supported by: NIH awards 1U18TR003795, 4U18TR003795, 1U01TR004083 and UL1 TR001860; UG3-OD023365; 1P30ES023513-01A1 [CED, NJK]; the Department of Veterans Affairs award I01 BX004965-01A1 [NJK, CED]; the University of California Tobacco-Related Disease Research Program award T31IR1614 [CED, NJK]; the Advanced Regenerative Manufacturing Institute, Inc. W911NF-17-3-0003 subaward T0173-B [CED]; and the National Science Foundation award 2200221 [CED]. Student support was provided by: NIH NHLBI T32 HL07013 [BDC]; US Department of Education Award P200A180054 [DTK]; and National Science Foundation Graduate Research Fellowship Program [LAS][34]. Part of this study was carried out at the UC Davis Center for Nano and Micro Manufacturing (CNM2). The contents of this manuscript are solely the responsibility of the authors and do not necessarily represent the official views of the funding agencies. This research was partially sponsored by the Office of the Secretary of Defense and was accomplished under Agreement Number W911NF-17-3-0003 [CED]. The views and conclusions contained in this document are those of the authors and should not be interpreted as representing the official policies, either expressed or implied, of the Office of the Secretary of Defense of the U.S. Government. The U.S. Government is authorized to reproduce and distribute reprints for Government purposes notwithstanding any copyright notation herein.

REFERENCES

1. Mandoj F; Nardis S; Di Natale C; Paolesse R, Porphyrinoid Thin Films for Chemical Sensing. In Encyclopedia of Interfacial Chemistry, Wandelt K, Ed. Elsevier: Oxford, 2018; pp 422–443.

Author Manuscript Author Manuscript Author Manuscript Author Manuscript

2. Kaniewska M; Trojanowicz M, Chapter 8 - Chiral Sensors Based on Molecularly Imprinted Polymers. In Molecularly Imprinted Sensors, Li S; Ge Y; Piletsky SA; Lunec J, Eds. Elsevier: Amsterdam, 2012; pp 175–194.

3. Pan TM; Mondal S, 13.07 - Structural Properties and Sensing Characteristics of Sensing Materials. In Comprehensive Materials Processing, Hashmi S; Batalha GF; Van Tyne CJ; Yilbas B, Eds. Elsevier: Oxford, 2014; pp 179–203.

4. Rudnitskaya A., Sensors | Biomimetic Sensor Arrays. In Encyclopedia of Analytical Science (Third Edition), Worsfold P; Poole C; Townshend A; Miró M, Eds. Academic Press: Oxford, 2019; pp 154–160.

5. Güntner AT; Abegg S; Königstein K; Gerber PA; Schmidt-Trucksäss A; Pratsinis SE, Breath Sensors for Health Monitoring. ACS Sens. 2019, 4 (2), 268–280. [PubMed: 30623644]

6. Fung S; LeVasseur MK; Rajapakse MY; Chew BS; Fung AG; McCartney MM; Kenyon NJ; Davis CE, Battery powered dual-polarity ion detector for trace chemical sensing. Sens. Actuators, A 2022, 338, 113442.

7. Simms LA; Borras E; Chew BS; Matsui B; McCartney MM; Robinson SK; Kenyon N; Davis CE, Environmental sampling of volatile organic compounds during the 2018 Camp Fire in Northern California. Journal of Environmental Sciences (Beijing, China) 2021, 103, 135–147.

8. Zamuruyev KO; Schmidt AJ; Borras E; McCartney MM; Schivo M; Kenyon NJ; Delplanque J-P; Davis CE, Power-efficient self-cleaning hydrophilic condenser surface for portable exhaled breath condensate (EBC) metabolomic sampling. J. Breath Res 2018, 12 (3), 036020. [PubMed: 29771240]

9. Schmidt AJ; Borras E; Nguyen AP; Yeap D; Kenyon NJ; Davis CE, Portable exhaled breath condensate metabolomics for daily monitoring of adolescent asthma. J. Breath Res 2020, 14 (2), 026001. [PubMed: 31344695]

10. Yeom J; Field CR; Bae B; Masel RI; Shannon MA, The design, fabrication and characterization of a silicon microheater for an integrated MEMS gas preconcentrator. J. Micromech. Microeng 2008, 18 (12), 125001.

11. Camara EHM; Breuil P; Briand D; de Rooij NF; Pijolat C, A micro gas preconcentrator with improved performance for pollution monitoring and explosives detection. Anal. Chim. Acta 2011, 688 (2), 175–182. [PubMed: 21334483]

12. Camara EHM; Breuil P; Briand D; Guillot L; Pijolat C; de Rooij NF, Micro gas preconcentrator in porous silicon filled with a carbon absorbent. Sens. Actuators, B 2010, 148 (2), 610–619.

13. van den Broek J; Mochalski P; Königstein K; Ting WC; Unterkofler K; Schmidt-Trucksäss A; Mayhew CA; Güntner AT; Pratsinis SE, Selective monitoring of breath isoprene by a portable detector during exercise and at rest. Sens. Actuators, B 2022, 357, 131444.

14. Wei-Hao Li M; Ghosh A; Venkatasubramanian A; Sharma R; Huang X; Fan X, High-sensitivity micro-gas chromatograph–photoionization detector for trace vapor detection. ACS Sens. 2021, 6 (6), 2348–2355. [PubMed: 34028248]

15. McCartney MM; Zrodnikov Y; Fung AG; LeVasseur MK; Pedersen JM; Zamuruyev KO; Aksenov AA; Kenyon NJ; Davis CE, An Easy to Manufacture Micro Gas Preconcentrator for Chemical Sensing Applications. ACS Sens 2017, 2 (8), 1167–1174. [PubMed: 28753000]

16. Fung AG; Rajapakse MY; McCartney MM; Falcon AK; Fabia FM; Kenyon NJ; Davis CE, Wearable Environmental Monitor To Quantify Personal Ambient Volatile Organic Compound Exposures. ACS Sens. 2019, 4 (5), 1358–1364. [PubMed: 31074262]

17. Rajapakse MY; Borras E; Fung AG; Yeap D; McCartney MM; Fabia FM; Kenyon NJ; Davis CE, An environmental air sampler to evaluate personal exposure to volatile organic compounds. Analyst (Cambridge UK) 2021, 146 (2), 636–645.

18. Trinh NN; Simms LA; Chew BS; Weinstein A; La Saponara V; McCartney MM; Kenyon NJ; Davis CE Glass-to-Glass Fusion Bonding Quality and Strength Evaluation with Time, Applied Force, and Heat Micromachines [Online], 2022.

19. Emergency Awards RADx-RAD: Screening for COVID-19 by Electronic-Nose Technology (SCENT) (U18 Clinical Trial Not Allowed). National Institute of Health: 2020.

20. Screening for Conditions by Electronic Nose Technology (SCENT) (U01 Clinical Trial Optional). National Institue of Health: 2021.

Author Manuscript Author Manuscript Author Manuscript Author Manuscript

21. Robin AK; Malte S-R; Bernd R; Oktavia O; Roman O; Norbert A In LIDE: high aspect ratio glass processing technology for the mass production of microfluidic devices for biomedical applications, Proc.SPIE, 2019; p 1087506.
22. Wolffenbuttel RF; Wise KD, Low-temperature silicon wafer-to-wafer bonding using gold at eutectic temperature. Sens. Actuators, A 1994, 43 (1), 223–229.
23. Berthold A; Nicola L; Sarro PM; Vellekoop MJ, Glass-to-glass anodic bonding with standard IC technology thin films as intermediate layers. Sens. Actuators, A 2000, 82 (1), 224–228.
24. Kaidatzis A; Psycharis V; Mergia K; Niarchos D, Annealing effects on the structural and electrical properties of sputtered tungsten thin films. Thin Solid Films 2016, 619, 61–67.
25. Lishan D; Mackenzie K; Fresina M; Wend D; Erickson J; Johnson D, Process Performance. Sigma 1, 1.5.
26. Mackenzie K; Lee J; Johnson D In Inductively-coupled plasma deposition of low temperature silicon dioxide and silicon nitride films for III–V applications, Proc. 30th Symp. State-of-the-Art Progr. Comp. Semicond, 1999; pp 1–12.
27. Lazerand T; Lishan D, Silicon Nitride for MEMS Applications: LPCVD and PECVD Process Comparison. MEMS Journal 2014.
28. Maracas GN; Edwards JL; Shiralagi K; Choi KY; Droopad R; Johs B; Woolam JA, In situ spectroscopic ellipsometry in molecular beam epitaxy. J. Vac. Sci. Technol. A 1992, 10 (4), 1832–1839.
29. Wei J; Xie H; Nai M; Wong C; Lee L, Low temperature wafer anodic bonding. J. Micromech. Microeng 2003, 13 (2), 217.
30. Lapadatu AC; Jakobsen H, Chapter 30 - Anodic Bonding. In Handbook of Silicon Based MEMS Materials and Technologies (Second Edition), Tilli M; Motooka T; Airaksinen V-M; Franssila S; Paulasto-Kröckel M; Lindroos V, Eds. William Andrew Publishing: Boston, 2015; pp 599–610.
31. Louter AJ; Van Doornmalen J; Vreuls JJ; Brinkman UAT, On-line solid-phase extraction-thermal desorption-gas chromatography with ion trap detection tandem mass spectrometry for the analysis of microcontaminants in water. J. High. Resolut. Chromatogr 1996, 19 (12), 679–685.
32. Demeestere K; Dewulf J; De Roo K; De Wispelaere P; Van Langenhove H, Quality control in quantification of volatile organic compounds analysed by thermal desorption–gas chromatography–mass spectrometry. J. Chromatogr. A 2008, 1186 (1-2), 348–357. [PubMed: 18062983]
33. Bruno P; Caputi M; Caselli M; De Gennaro G; De Rienzo M, Reliability of a BTEX radial diffusive sampler for thermal desorption: field measurements. Atmos. Environ 2005, 39 (7), 1347–1355.
34. Chew BS; Pimentel Contreras R; McCartney MM; Borras E; Kenyon NJ; Davis CE, A low cost, easy-to-assemble, open-source modular mobile sampler design for thermal desorption analysis of breath and environmental VOCs. J. Breath Res 2022, 16 (3), 036005.

Author Manuscript Author Manuscript Author Manuscript Author Manuscript

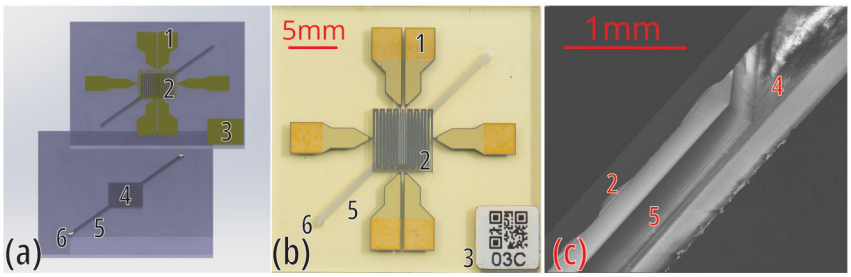

Figure 1.

A micro preconcentrator displayed in three formats. (a) A 3D rendering of the design with exploded top and bottom halves typically bonded together, (b) a realized fabricated device used in this study, (c) SEM of a micro preconcentrator cross section cut with a dicing saw down the line of the channel. Displayed are: (1) Electrical contact pads used to interface the device with driving electronics, (2) metal traces for the heater and RTD features, (3) metal pad and QR code used for identification and scanning chip history, (4) etched sorbent cavity, (5) etched micro channels, (6) through glass vias used to introduce and desorb chemical samples to the chip.

Author Manuscript Author Manuscript Author Manuscript Author Manuscript

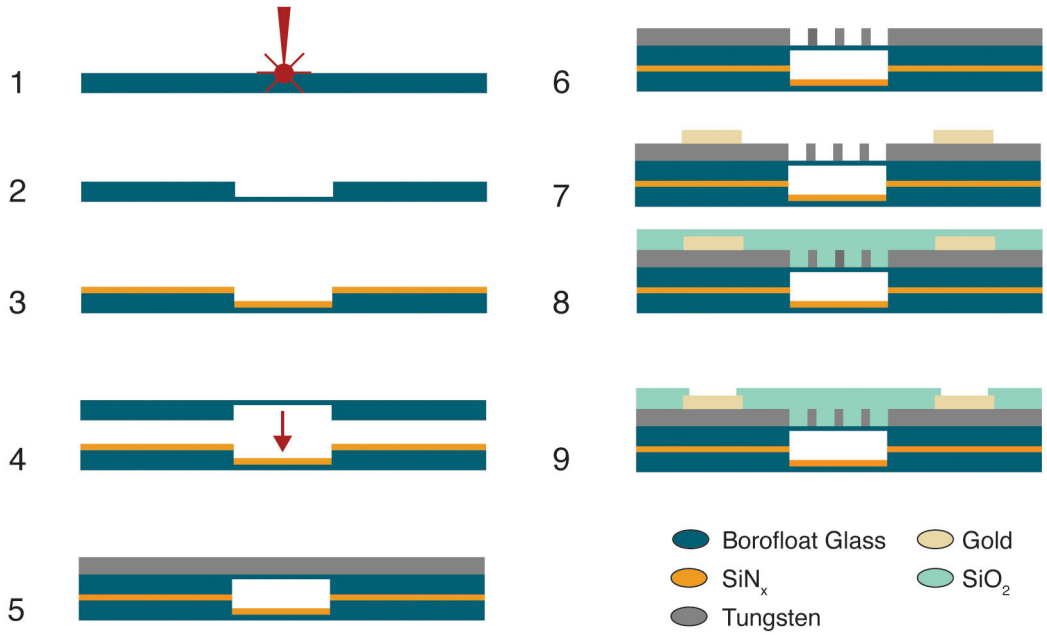

Figure 2.

µPC chip fabrication process. (1) Laser initiation of a Borofloat33 substrate followed by; (2) selective wet etching in HF; (3) an intermediate SiNx layer is deposited with PECVD to assist with glass-glass anodic bonding; (4) complimentary wafers are glass-glass bonded to form the cavity and channels; (5,6) a layer of Chromium-Tungsten-Chromium is deposited and etched to form the heater and RTD traces; (7) gold is electron-beam evaporated onto the contact pads; (8,9) SiO_2 passivation layer is deposited with PECVD and etched back to protect the heater and RTD traces.

Author Manuscript Author Manuscript Author Manuscript Author Manuscript

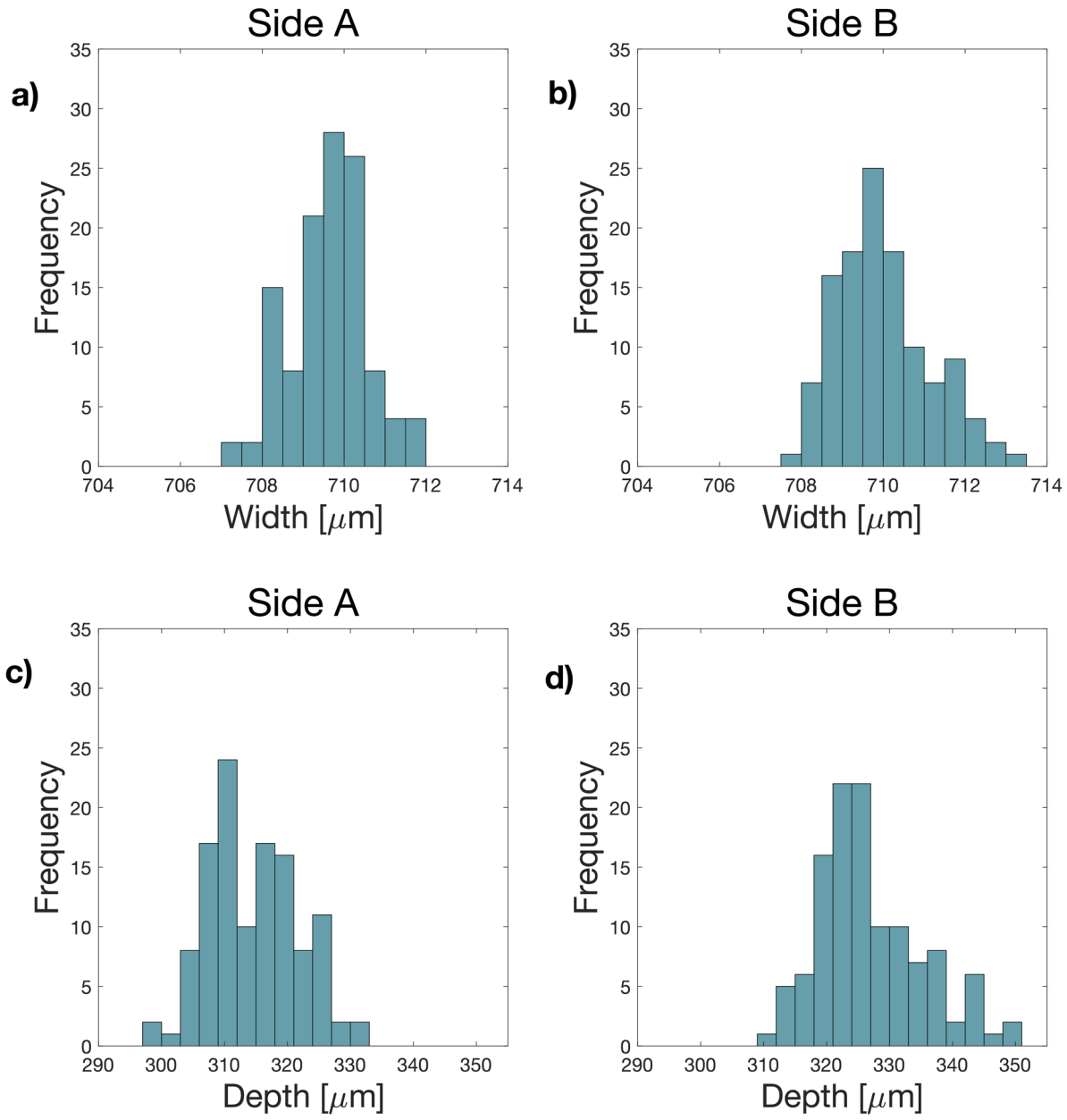

Figure 3.

Distributions from etching process (n = 118) for channel dimensions of (a) side A width; (b) side B width; (c) side A depth; (d) side B depth.

Author Manuscript Author Manuscript Author Manuscript Author Manuscript

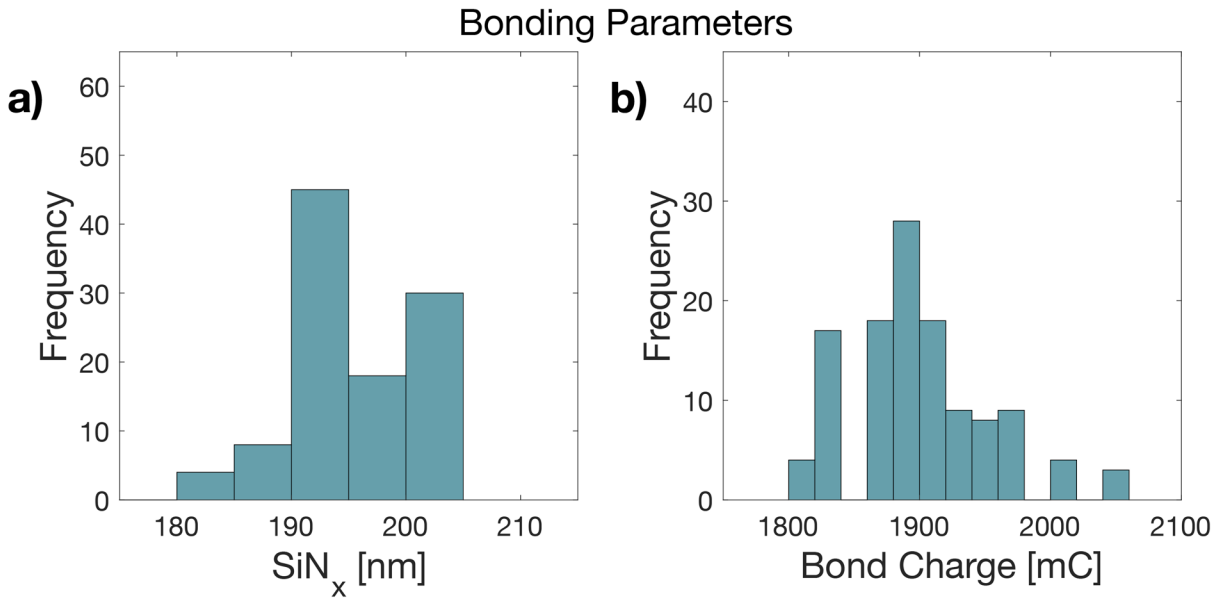

Figure 4.
Distribution from bonding parameters (n = 27) for (a) SiNx layer thickness; (b) Anodic bond max charge.

Author Manuscript Author Manuscript Author Manuscript Author Manuscript

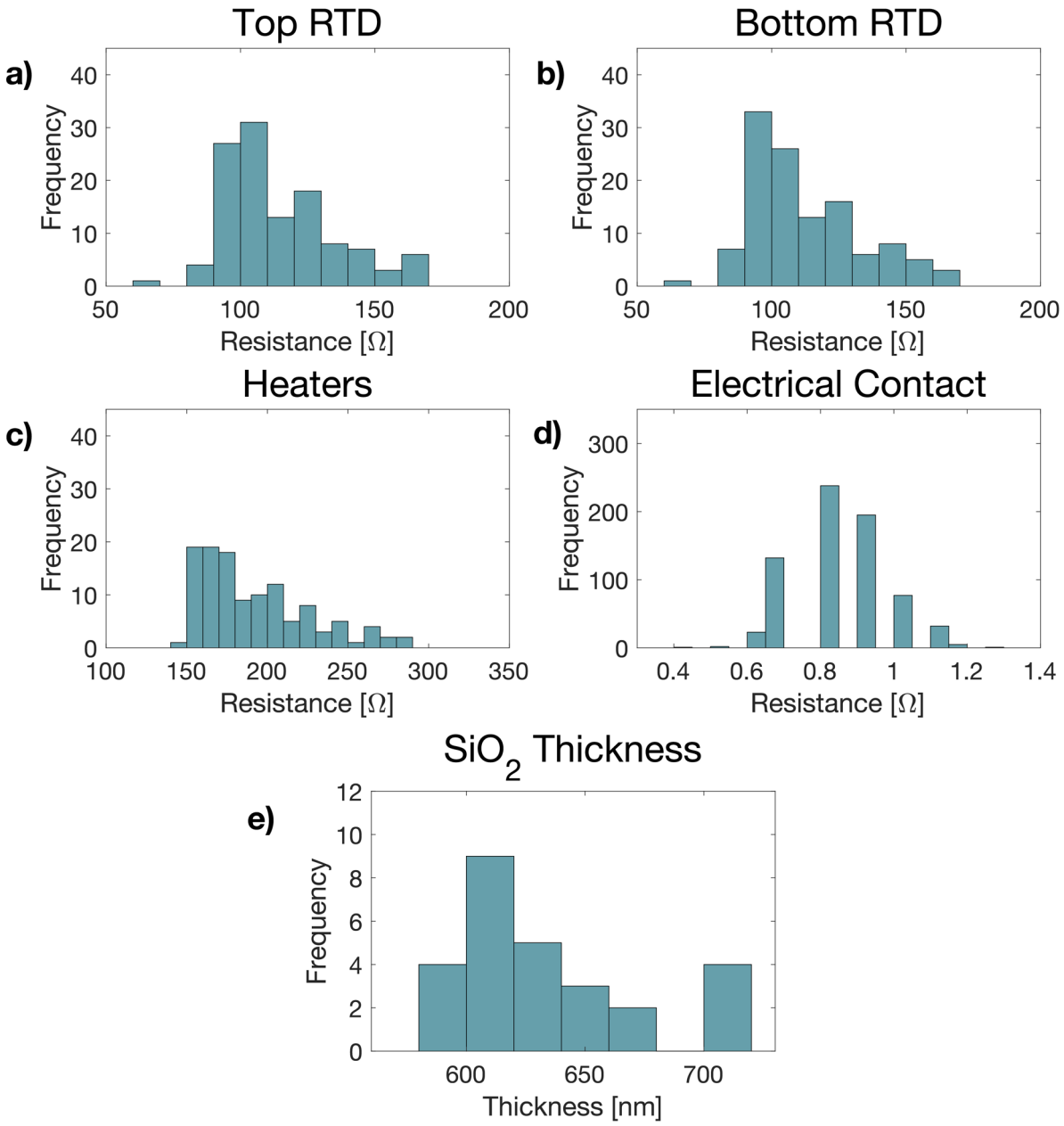

Figure 5.

Distributions of heater manufacturing parameters after Cr-W-Cr metal deposition, etching processes and SiO_2 passivation for (a) Top RTD (n = 118); (b) Bottom RTD (n = 118); (c) Heater (n = 118); and (d) Electrical Contact from post gold deposition on pads (n = 708); (e) Distribution of SiO_2 passivation layer thickness deposited (n = 27).

Author Manuscript Author Manuscript Author Manuscript Author Manuscript

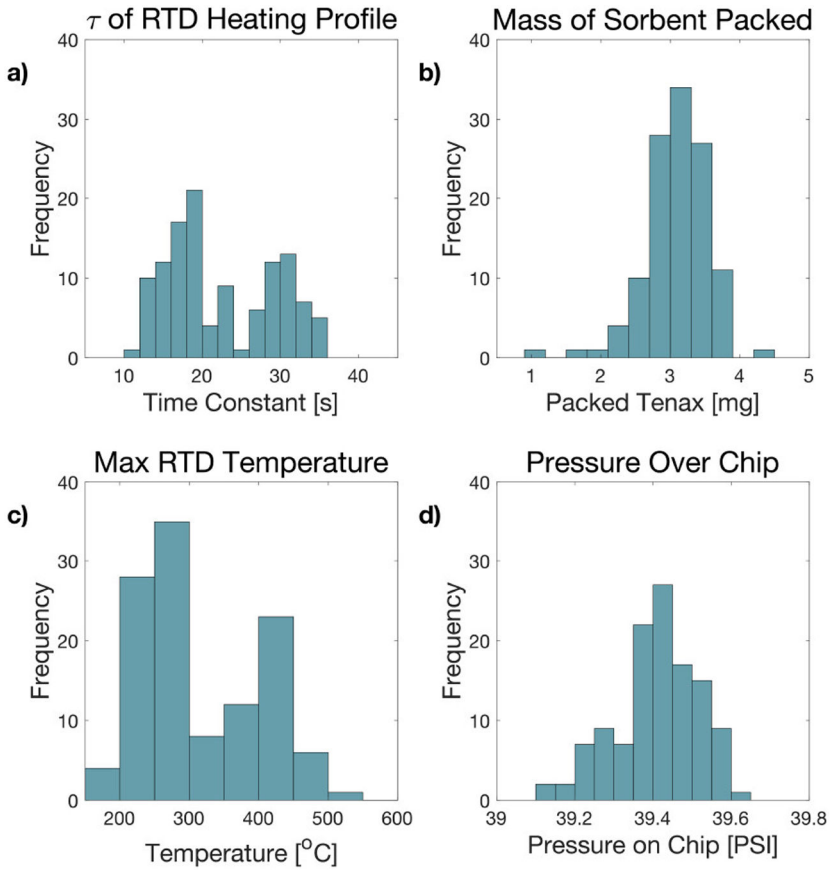

Figure 6.

Distribution of thermal desorption parameters during GC-FID chemical testing ($n = 118$) for (a) τ of RTD heating profile; (b) Mass of sorbent; (c) Maximum RTD temperature; (d) Pressure over chip.

Author Manuscript Author Manuscript Author Manuscript Author Manuscript

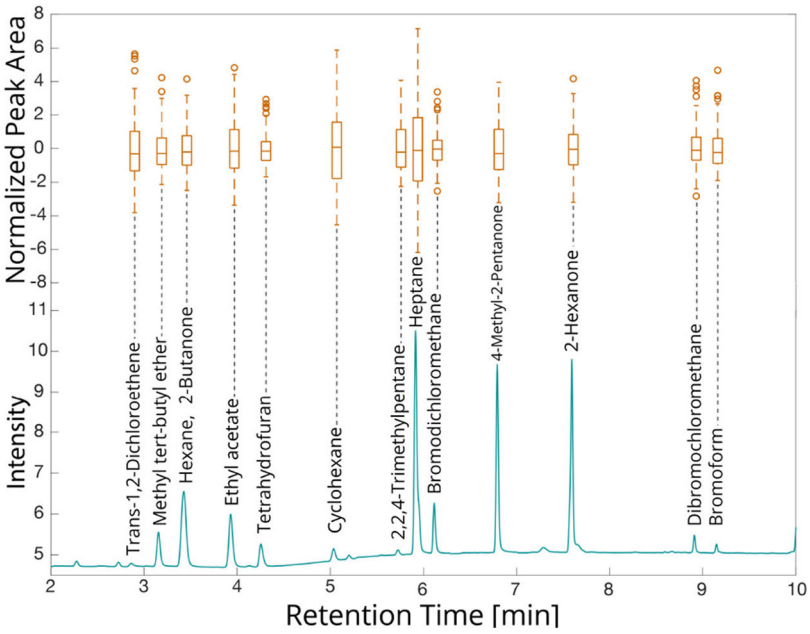

Figure 7:

Gas chromatography flame ionization chromatogram (GC-FID) from a preconcentrated VOC gas mixture. The bottom shows an example chromatogram from preconcentrator serial number 03C with individual compound peaks identified. The top box and whisker plot each chemical compound's mean centered signal distributions from all chips (n = 118) normalized to the standard deviation of the measurement variation study.

Author Manuscript Author Manuscript Author Manuscript Author Manuscript

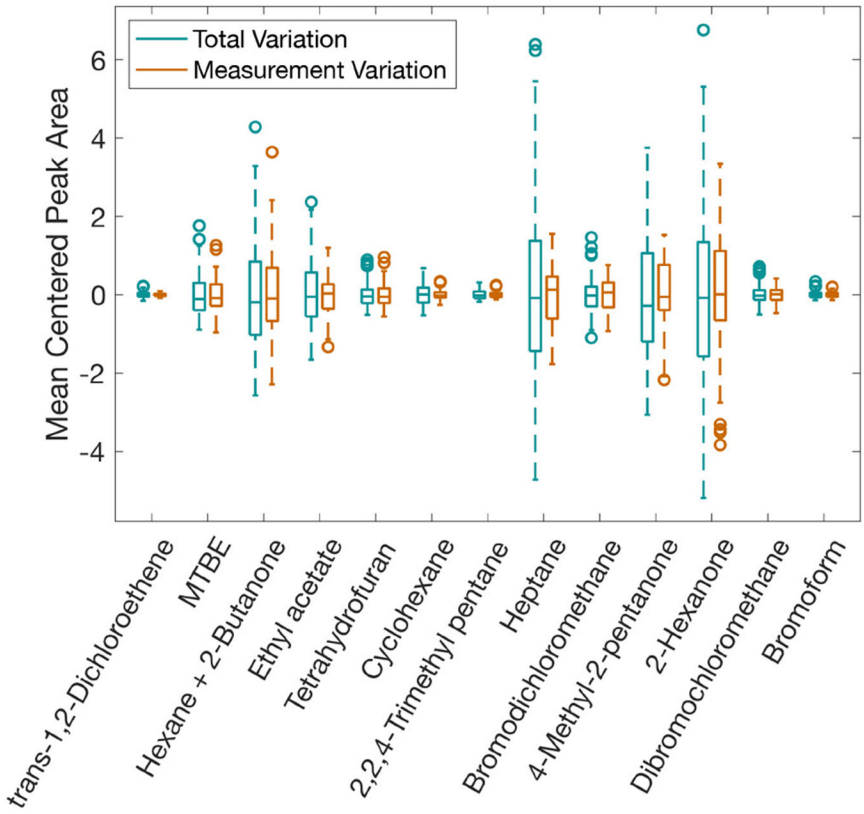

Figure 8:

Comparison of the mean centered GC-FID peak area box and whisker plots from the main (n=118) study to the measurement variation study (n=35 pairs) for each chemical compound.

Author Manuscript Author Manuscript Author Manuscript Author Manuscript

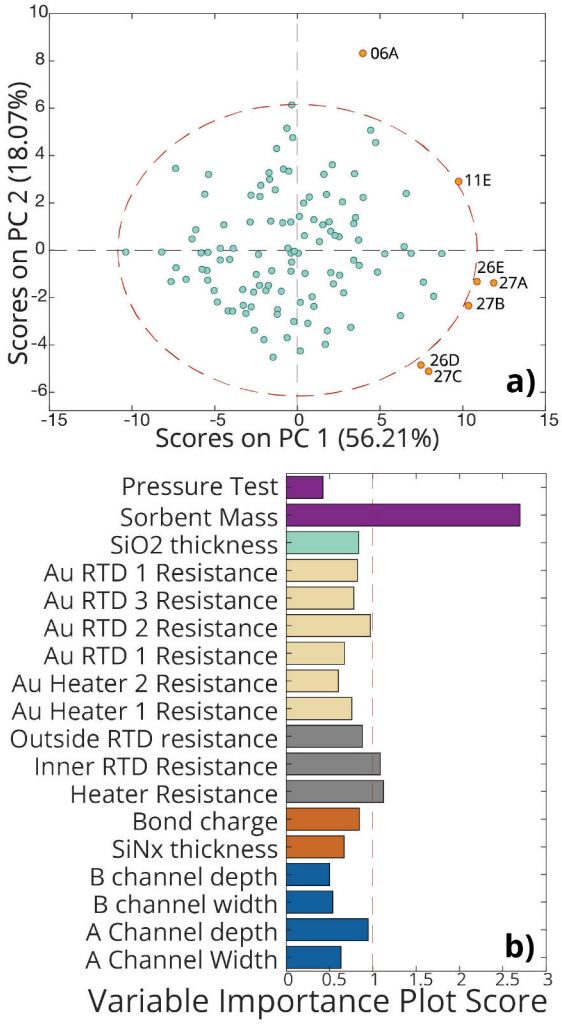

Figure 9:

Results from principal component analysis and partial least squared regression modeling; a) PC1 and PC2 scores for all chemically tested μPC chips. Blue dots represent μPC chips that fell within the 95% confidence interval — red dashed line — while orange markers represent potential outlier chips, labeled with the chip serial number. b) Variable importance scores obtained by PLS regression. Variables with a score greater than one indicate manufacturing parameters predictive of device performance. Higher scores have stronger correlations.